Numerical Implementation of Boundary Conditions for Finite Difference Method on Staggered Grid for Wave Propagation in Saturated Porous Medium

Galina Reshetova[1(✉)] and Evgeniy Romenski[2]

[1] Institute of Computational Mathematics and Mathematical Geophysics SB RAS, Novosibirsk 630090, Russia
kgv@nmsf.sscc.ru

[2] Sobolev Institute of Mathematics SB RAS, Novosibirsk 630090, Russia
evrom@math.nsc.ru

Abstract. This paper presents a numerical implementation of boundary conditions in the finite difference staggered grid method for a Hyperbolic Thermodynamically Compatible (HTC) model of wavefields simulations in a three-phase model of a deformable porous medium saturated with a mixture of two fluids. A number of test problems on the propagation of high-frequency waves have been solved and it has been shown that the developed numerical method is applicable to non-stationary processes in domains of complex structure. The method can also be applied to obtain a steady-state solution of the equilibrium equations of a saturated porous medium by solving a nonstationary system.

Keywords: Wavefield simulation · Fluid saturated porous medium · Boundary conditions · Staggered grid finite difference scheme

1 Introduction

In recent years, in connection with the development of new technologies and the need to intensify the development of natural resources, there is a need to model wave processes in porous media. The most widely accepted model for this is the Biot model [1,2] and its generalizations (see [3] and references therein), which are generally accepted in the geophysical community. However, this model has significant limitations in its applicability, namely, it is unclear how to generalize it to the case when the saturating fluid is multiphase, when the medium is subject to finite deformations, etc.

This paper is based on the use of a Hyperbolic Thermodynamically Compatible (HTC) model for simulations of wavefields in a saturated deformable porous medium, which was proposed and studied in [4–8]. These equations are derived from the general multiphase HTC model, which in turn is obtained on the basis of the theory of HTC equations of continuum mechanics (see [11] and references

© The Author(s), under exclusive license to Springer Nature Switzerland AG 2026
O. Gervasi et al. (Eds.): ICCSA 2025 Workshops, LNCS 15888, pp. 359–375, 2026.
https://doi.org/10.1007/978-3-031-97596-7_24

therein). The governing equations of the model form a first-order hyperbolic system and, due to their structure, allow the use of an effective finite difference method on a staggered grid. Our previous studies of wavefields in domains of complex structure were performed for unbounded domains using the Perfectly Matched Layers (PML) method. In fact, to solve many practical problems, it is necessary to study wavefields in bounded domains, that is, to use boundary conditions. The aim of this work is the numerical implementation of boundary conditions for the finite difference method on a staggered grid.

The rest of the paper is organized as follows. In Sect. 2 the governing equations for wave propagation in the porous medium saturated with the mixture of two fluids are formulated and boundary conditions, which are used in the numerical test problems are presented. Section 3 presents solutions to a series of test problems, including a plane wave propagating from a boundary, the interaction of a plane wave with an inclusion, and finding a steady-state solution of a medium in equilibrium by solving non-stationary equations. Finally, the Appendix provides a description of the finite difference scheme used in the calculations on a staggered grid.

2 Governing Equations for Wavefields in a Porous Medium Saturated with a Two-Phase Fluid

2.1 Governing Equations of the Model

To model wavefields in a deformed porous medium saturated with a mixture of two fluids (in our case the gas-liquid mixture), we use the Hyperbolic Thermodynamically Compatible (HTC) model [8]. The system of governing equations presented below can be obtained using a general multiphase model of a mixture of liquids saturating a deformed porous medium. The equations of this general model are hyperbolic, and its solutions satisfy the laws of thermodynamics (conservation of energy and increase in entropy). The simplified linear model that we use in this paper is also hyperbolic and satisfies the thermodynamic law of energy dissipation [8].

Let us assume that the mixture of fluids consists of two liquids with numbers 1 and 2, and that the deformed skeletal phase has number 3. Then the porosity is equal to $\phi = 1 - \alpha_1^0 - \alpha_2^0$. Assume also that the constant phase mass densities are ρ_1^0, ρ_2^0, ρ_3^0, and then the mass density of the mixture is $\rho_0 = \alpha_1^0\rho_1^0 + \alpha_2^0\rho_2^0 + \alpha_3^0\rho_3^0$. Let us formulate a three-dimensional version of governing equations. The complete set of state variables for the description of the medium consists of the velocity vector of the mixture V^i, $i = 1, 2, 3$, the velocities of movement of the first and second phases relative to the third phase (relative velocities) W_1^i, $i = 1, 2, 3$ and W_2^i, $i = 1, 2, 3$, shear stress (deviatoric part of the stress tensor) Σ_{ik}, $i, k = 1, 2, 3$, and pressure P.

Using the above notations, we formulate a closed system for wavefields that includes equations for the mixture velocity and relative velocities, as well as for pressure and shear stress, and has the form

$$\rho_0 \frac{\partial V^i}{\partial t} + \frac{\partial P}{\partial x_i} - \frac{\partial \Sigma_{ik}}{\partial x_k} = \Phi^i, \tag{1a}$$

$$\frac{\partial W_1^i}{\partial t} + \left(\frac{1}{\rho_1^0} - \frac{1}{\rho_3^0}\right)\frac{\partial P}{\partial x_i} = -\Lambda_1^i, \tag{1b}$$

$$\frac{\partial W_2^i}{\partial t} + \left(\frac{1}{\rho_2^0} - \frac{1}{\rho_3^0}\right)\frac{\partial P}{\partial x_i} = -\Lambda_2^i, \tag{1c}$$

$$\frac{\partial P}{\partial t} + K\frac{\partial V^k}{\partial x_k} + K_1'\frac{\partial W_1^k}{\partial x_k} + K_2'\frac{\partial W_2^k}{\partial x_k} = 0, \tag{1d}$$

$$\frac{\partial \Sigma_{ik}}{\partial t} - \mu\left(\left(\frac{\partial V^i}{\partial x_k} + \frac{\partial V^k}{\partial x_i}\right) - \frac{2}{3}\delta_{ik}\left(\frac{\partial V^1}{\partial x_1} + \frac{\partial V^2}{\partial x_2} + \frac{\partial V^3}{\partial x_3}\right)\right) = -\frac{\Sigma_{ik}}{\tau}, \tag{1e}$$

Here, $K = \left(\frac{\alpha_1^0}{K_1} + \frac{\alpha_2^0}{K_2} + \frac{\alpha_3^0}{K_3}\right)^{-1}$ is the bulk modulus of the three-phase mixture, where K_1, K_2, K_3 are the phase bulk moduli. $K_a' = (\alpha_a^0 - c_a^0)K, (a = 1, 2)$, where $c_1^0 = \alpha_1^0\rho_1^0/\rho^0$, $c_2^0 = \alpha_2^0\rho_2^0/\rho^0$ are the mass fractions of fluids, $\mu = c_1^0\mu_1 + c_2^0\mu_2 + c_3^0\mu_3$ is the shear modulus of the mixture and μ_1, μ_2, μ_3 are the shear moduli of the phases. In addition, we assume that the shear moduli of the liquids are zero, which means that $\mu = c_3^0\mu_3$.

The equations have right-hand sides that are responsible for external forces or processes related to internal interactions between phases. For example, the term Φ^i in equation (1a) is responsible for the sources of external forces that can generate seismic waves within the porous medium. The terms Λ_1^i, Λ_2^i in the equations (1b), (1c) for relative velocities and Σ_{ij}/τ in the equation (1e) for shear stress describe interfacial friction and shear stress relaxation respectively.

The total stress tensor of the mixture can be computed as $\sigma_{ik} = \Sigma_{ik} - P$ and is connected with the total strain tensor of the mixture ε_{ik} via Hooke's law:

$$\sigma_{ik} = \lambda(\varepsilon_{11} + \varepsilon_{22} + \varepsilon_{33})\delta_{ik} + 2\mu\varepsilon_{ik}. \tag{2}$$

The shear stress and pressure are connected with the strain tensor as

$$\Sigma_{ik} = 2\mu\left(\varepsilon_{ik} - \delta_{ik}\frac{(\varepsilon_{11} + \varepsilon_{22} + \varepsilon_{33})}{3}\right), \quad P = -K(\varepsilon_{11} + \varepsilon_{22} + \varepsilon_{33}). \tag{3}$$

Here the bulk modulus K and shear modulus μ of the mixture are defined above, and Lame constant λ can be computed with the use of the relation $K = \lambda + \frac{2}{3}\mu$.

The system(1) is hyperbolic, and in the one-dimensional case its characteristic velocities, equal to the velocities of two longitudinal waves (fast and slow

compression waves), can be calculated by the formula

$$C_1 = \frac{1}{\sqrt{2\rho_0}}\sqrt{\left(\tilde{K} + \frac{\rho_0 Q}{\rho_1^0\rho_2^0\rho_3^0}\right) + \sqrt{\left(\tilde{K} + \frac{\rho_0 Q}{\rho_1^0\rho_2^0\rho_3^0}\right)^2 + 4(K-\tilde{K})\frac{\rho_0 Q}{\rho_1^0\rho_2^0\rho_3^0}}} \quad (4)$$

$$C_2 = \frac{1}{\sqrt{2\rho_0}}\sqrt{\left(\tilde{K} + \frac{\rho_0 Q}{\rho_1^0\rho_2^0\rho_3^0}\right) - \sqrt{\left(\tilde{K} + \frac{\rho_0 Q}{\rho_1^0\rho_2^0\rho_3^0}\right)^2 + 4(K-\tilde{K})\frac{\rho_0 Q}{\rho_1^0\rho_2^0\rho_3^0}}} \quad (5)$$

and the shear wave can be calculated by the formula

$$C_3 = \sqrt{\frac{\mu}{\rho_0}}, \quad (6)$$

where $\tilde{K} = K + \frac{4}{3}\mu$, $Q = \rho_2^0(\rho_3^0 - \rho_1^0)K_1' + \rho_1^0(\rho_3^0 - \rho_2^0)K_2'$.

In [8] it was shown that the solutions of system (1) admit the additional energy dissipation law

$$\frac{\partial \mathcal{E}}{\partial t} + \frac{\partial \Pi_k}{\partial x_k} = -\mathcal{Q}, \quad (7)$$

where the total energy $\mathcal{E}$ of the porous medium is equal to

$$\mathcal{E} = \rho_0\frac{V^iV^i}{2} + \frac{\rho_0}{2}\sum_{a=1}^{2}c_a^0\sum_{k=1}^{3}(W_a^k)^2 - \frac{\rho_0}{2}\sum_{k=1}^{3}\left(\sum_{a=1}^{2}c_a^0W_a^k\right)^2 + \frac{1}{2K}P^2 + \frac{\Sigma_{ij}\Sigma_{ji}}{4\mu}, \quad (8)$$

and $\Pi_k = PV^k + \sum_{a=1}^{2}(\alpha_a^0 - c_a^0)PW_a^k - \Sigma_{ik}V^i$ is the energy flux and $\mathcal{Q} = \sum_{a=1}^{2}\mathcal{E}_{W_a^i}\Lambda_a^i + \frac{1}{\mu\tau}\Sigma_{ij}\Sigma_{ji}$ is the energy loss. Here, summation over repeating indices i, j is assumed.

Note that when solving the problem in the two-dimensional case in the plane x_1, x_2, the component of the deviator Σ_{33} can be non-zero and is found from the identity $\Sigma_{11} + \Sigma_{22} + \Sigma_{33} = 0$.

Note also that in all test cases below, we do not take into account dissipative source terms (interfacial friction and relaxation of shear stress), setting $\Lambda_1^i = 0$, $\Lambda_2^i = 0$, $\tau = \infty$.

2.2 Boundary Conditions

Let us consider the most common case of boundary conditions, when stresses are defined on the boundary. The system (1) is hyperbolic, so, according to the theory, the number of boundary conditions should coincide with the number of characteristics going from the boundary into the domain. The solutions of the equations(1) are characterised by three velocities, corresponding to two compression waves (fast and slow) and a shear wave. This means that we must define three boundary conditions. We consider two conditions with given normal and shear stresses, as well as the condition of no flow along the normal to the boundary.

If $\mathbf{n}$ is the normal vector to the boundary, and $\sigma = \mathbf{\Sigma} - P\mathbf{I}$ is the total stress tensor, then the boundary conditions for the stresses read as

$$(\sigma, \mathbf{n}) = \mathbf{F}(t), \tag{9}$$

where in the two-dimensional case $\mathbf{F}(t) = (F^1(t), F^2(t))^T$ and $F^1(t), F^2(t)$ are given functions. In component form (9) reads as $\sigma_n = F^1(t)$, $\sigma_t = F^2(t)$, where σ_n, σ_t are normal and tangential stresses. To set the no-flow condition, it is sufficient to set one relative velocity to zero, and the equality of the second relative velocity to zero follows from the equations (1b) and (1c). We set the no-flow condition as

$$(\mathbf{W_1}, \mathbf{n}) = 0, \tag{10}$$

which automatically implies $(\mathbf{W_2}, \mathbf{n}) = 0$ and we will add this to the list of boundary conditions in the finite difference scheme.

In the numerical test cases presented below we consider the rectangular domain $(x, y) \in [-a, a] \times [-b, b]$ with the following boundary conditions

$$\sigma_{11}|_{x=-a} = F_1^1(t),\ \sigma_{12}|_{x=-a} = F_1^2(t),\ W_1^1|_{x=-a} = 0,\ W_2^1|_{x=-a} = 0, \tag{11}$$

$$\sigma_{11}|_{x=a} = F_2^1(t),\ \sigma_{12}|_{x=a} = F_2^2(t),\ W_1^1|_{x=a} = 0,\ W_2^1|_{x=a} = 0 \tag{12}$$

$$\sigma_{22}|_{y=-b} = F_3^1(t),\ \sigma_{12}|_{y=-b} = F_3^2(t),\ W_1^2|_{y=-b} = 0,\ W_2^2|_{y=-b} = 0, \tag{13}$$

$$\sigma_{22}|_{y=b} = F_4^1(t),\ \sigma_{12}|_{y=b} = F_4^2(t),\ W_1^2|_{y=b} = 0,\ W_2^1|_{y=b} = 0. \tag{14}$$

3 Numerical Simulations

In this section, we perform a numerical analysis of the key characteristics of small-amplitude wave propagation in a porous medium containing a saturated compressible mixture of two fluids. To numerically solve the system of equations (1), we use finite difference methods on a staggered grid [12–14] with a fourth order accuracy in space and a second order accuracy in time.

3.1 Finite Difference Approximation

The derivation of finite difference scheme for solving system (1) using the staggered grid follows a similar approach to that in [12,13]. The staggered grid finite difference method is based on the finite volume discretization technique discussed in particular in [14] and is often used for systems of equations derived from physical conservation principles. A major advantage of this method is that it avoids the need to approximate the fluxes during the computation, as these values are predetermined, thereby increasing both the efficiency and reliability of the approach. Within this framework, we specify the deviatoric stresses, presure and velocities at distinct grid points in both space and time, achieving a fourth order accuracy approximation with a minimum difference scheme stencil.

First, we construct a grid within the (t, x_1, x_2) time-space framework, with integer nodes at $t^n = n\Delta t$, $x_1^i = i\Delta x_1$, $x_2^j = j\Delta x_2$ and with semi-integer nodes

at $t^{n+1/2} = (n+1/2)\Delta t$, $x_1^{i+1/2} = (i+1/2)\Delta x_1$, $x_2^{j+1/2} = (j+1/2)\Delta x_2$. Here Δt and Δx_1, Δx_2 denote the grid spacing in time and space respectively.

We assume that the material parameters remain constant within each grid cell $[x_1^{i-1/2}, x_1^{i+1/2}] \times [x_2^{j-1/2}, x_2^{j+1/2}]$, allowing potential discontinuities at the grid boundaries. The mixture velocity V^1 and the relative velocities W_1^1 and W_2^1 are defined at the nodes $(n, i+1/2, j)$ and are denoted as $(V^1)^n_{i+1/2,j}$, $(W_1^1)^n_{i+1/2,j}$, and $(W_2^1)^n_{i+1/2,j}$. Similarly, the velocities V^2, W_1^2 and W_2^2 are defined at the nodes $(n, i, j+1/2)$ and are denoted as $(V^2)^n_{i,j+1/2}$, $(W_1^2)^n_{i,j+1/2}$ and $(W_2^2)^n_{i,j+1/2}$.

The pressure and diagonal deviatoric stresses are assigned to the integer nodes in space and semi-integer nodes in time at $(n+1/2, i, j)$, denoted as $(P)^{n+1/2}_{i,j}$, $(\Sigma_{11})^{n+1/2}_{i,j}$ and $(\Sigma_{22})^{n+1/2}_{i,j}$. The shear stress is assigned to the nodes $(n+1/2, i+1/2, j+1/2)$ and denoted as $(\Sigma_{12})^{n+1/2}_{i+1/2,j+1/2}$. The spatial configuration of the nodes on the staggered grid is shown in Fig. 1.

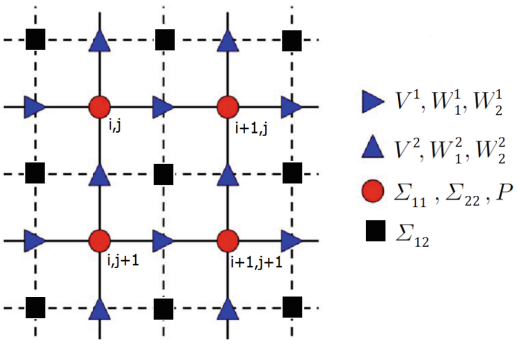

Fig. 1. The relative position of deviatoric stresses, pressure, mixture velocities and relative velocities on the staggered grid.

For compactness, we introduce a few notations for a discrete function $f^n_{i,j} = f(t^n, x_1^i, x_2^j)$:

– Second-order central difference operators

$$D_t[f]^n_{i,j} = \frac{(f)^{n+1/2}_{i,j} - (f)^{n-1/2}_{i,j}}{\Delta t}, \qquad A_t[f]^n_{i,j} = \frac{(f)^{n+1/2}_{i,j} + (f)^{n-1/2}_{i,j}}{2}, \quad (15)$$

– Fourth-order central difference operators (Levander stencil)

$$D_1[f]^n_{i,j} = \frac{1}{\Delta x_1}\left\{\frac{9}{8}\left((f)^n_{i+1/2,j} - (f)^n_{i-1/2,j}\right) - \frac{1}{24}\left((f)^n_{i+3/2,j} - (f)^n_{i-3/2,j}\right)\right\}, \quad (16)$$

$$D_2[f]^n_{i,j} = \frac{1}{\Delta x_2}\left\{\frac{9}{8}\left((f)^n_{i,j+1/2} - (f)^n_{i,j-1/2}\right) - \frac{1}{24}\left((f)^n_{i,j+3/2} - (f)^n_{i,j-3/2}\right)\right\}, \quad (17)$$

– Volumetric arithmetic averaging

$$\langle f\rangle^n_{i+1/2,j} = (f^n_{i,j} + f^n_{i+1,j})/2, \qquad \langle f\rangle^n_{i,j+1/2} = (f^n_{i,j} + f^n_{i,j+1})/2, \tag{18}$$

– Harmonic averaging by [15]

$$\{f\}^n_{i+1/2,j+1/2} = \left[\frac{1}{4}\left(\frac{1}{f^n_{i,j}} + \frac{1}{f^n_{i+1,j}} + \frac{1}{f^n_{i,j+1}} + \frac{1}{f^n_{i+1,j+1}}\right)\right]^{-1}. \tag{19}$$

Using these notation, the finite difference equations can be written as

$$\begin{aligned} D_t[V^1]^{n-1/2}_{i+1/2,j} &= -1/\left\langle\rho^0\right\rangle_{i+1/2,j} D_1[P]^{n-1/2}_{i+1/2,j} + \\ &+1/\left\langle\rho^0\right\rangle_{i+1/2,j}\left(D_1[\Sigma_{11}]^{n-1/2}_{i+1/2,j} + D_2[\Sigma_{12}]^{n-1/2}_{i+1/2,j}\right) + (\Phi^1)^{n-1/2}_{i+1/2,j}, \end{aligned}$$

$$\begin{aligned} D_t[V^2]^{n-1/2}_{i,j+1/2} &= -1/\left\langle\rho^0\right\rangle_{i,j+1/2} D_2[P]^{n-1/2}_{i,j+1/2} + \\ &+1/\left\langle\rho^0\right\rangle_{i,j+1/2}\left(D_1[\Sigma_{12}]^{n-1/2}_{i,j+1/2} + D_2[\Sigma_{22}]^{n-1/2}_{i,j+1/2}\right) + (\Phi^2)^{n-1/2}_{i,j+1/2}, \end{aligned}$$

$$D_t[W^1_1]^{n-1/2}_{i+1/2,j} = -\left\langle 1/\rho^0_1 - 1/\rho^0_3\right\rangle_{i+1/2,j} D_1[P]^{n-1/2}_{i+1/2,j} - A_t[\Lambda^1_1]^{n-1/2}_{i+1/2,j},$$

$$D_t[W^1_2]^{n-1/2}_{i+1/2,j} = -\left\langle 1/\rho^0_2 - 1/\rho^0_3\right\rangle_{i+1/2,j} D_1[P]^{n-1/2}_{i+1/2,j} - A_t[\Lambda^1_2]^{n-1/2}_{i+1/2,j},$$

$$D_t[W^2_1]^{n-1/2}_{i,j+1/2} = -\left\langle 1/\rho^0_1 - 1/\rho^0_3\right\rangle_{i,j+1/2} D_2[P]^{n-1/2}_{i,j+1/2} - A_t[\Lambda^2_1]^{n-1/2}_{i,j+1/2},$$

$$D_t[W^2_2]^{n-1/2}_{i,j+1/2} = -\left\langle 1/\rho^0_2 - 1/\rho^0_3\right\rangle_{i,j+1/2} D_2[P]^{n-1/2}_{i,j+1/2} - A_t[\Lambda^2_2]^{n-1/2}_{i,j+1/2},$$

$$\begin{aligned} D_t[P]^n_{i,j} &= -(K)_{i,j}\left(D_1[V^1]^n_{i,j} + D_2[V^2]^n_{i,j}\right) - \\ &-(K'_1)_{i,j}\left(D_1[W^1_1]^n_{i,j} + D_2[W^2_1]^n_{i,j}\right) - (K'_2)_{i,j}\left(D_1[W^1_2]^n_{i,j} + D_2[W^2_2]^n_{i,j}\right), \end{aligned}$$

$$D_t[\Sigma_{11}]^n_{i,j} = (\mu)_{i,j}\left(\tfrac{4}{3}D_1[V^1]^n_{i,j} - \tfrac{2}{3}D_2[V^2]^n_{i,j}\right) - (1/\tau)_{i,j} A_t[\Sigma_{11}]^n_{i,j},$$

$$D_t[\Sigma_{22}]^n_{i,j} = (\mu)_{i,j}\left(\tfrac{4}{3}D_2[V^2]^n_{i,j} - \tfrac{2}{3}D_1[V^1]^n_{i,j}\right) - (1/\tau)_{i,j} A_t[\Sigma_{22}]^n_{i,j},$$

$$\begin{aligned} D_t[\Sigma_{12}]^n_{i+1/2,j+1/2} &= \{\mu\}_{i+1/2,j+1/2}\left(D_1[V^2]^n_{i+1/2,j+1/2} + D_2[V^1]^n_{i+1/2,j+1/2}\right) - \\ &- \{1/\tau\}_{i+1/2,j+1/2} A_t[\Sigma_{12}]^n_{i+1/2,j+1/2}. \end{aligned}$$

The scheme obtained is an explicit finite difference scheme of fourth-order accuracy in time and space for a homogeneous elastic medium. The stability conditions and dispersion properties can be found in [12].

3.2 Approximation of Boundary Conditions on Staggered Grid

The setting of boundary conditions is often problem-specific and can vary depending on the physical nature of the process being modelled. For example,

in geophysical problems when modelling underground aquifers in the context of oil or gas field development, constant wall pressure is required.

When approximating boundary conditions by finite differences on staggered meshes, it is important to note that some variables may be specified at integer nodes and others at semi-integer nodes. It is known that such a shift of nodes and variables significantly affects the accuracy and stability of the numerical solution, and also provides a more accurate representation of the physical processes occurring at the boundaries of the computational domain.

For example, the values of physical parameters such as pressure or temperature are often specified in integer mesh nodes. This approach ensures that conditions at the boundaries are accurately accounted for, contributing to a more accurate representation of values at points where transitions occur. Conversely, components such as velocities or gradients associated with flow may be specified in semi-integer nodes. This is because such nodes facilitate a more accurate approximation of derivatives and interactions between neighboring nodes, which is particularly important for dynamic processes.

Approximation of boundary conditions using both integer and semi-integer nodes allows us to take into account various physical processes occurring on the boundary of the region, while ensuring the required accuracy of calculations by the difference scheme.

The approximation of the boundary conditions (11)–(14) on the staggered grid introduced in Sect. 3.1 is shown in the Fig. 2. The nodes where specific boundary conditions occur are highlighted in red.

Below, three test problems are considered using the developed finite difference method on a staggered grid.

3.3 Test 1

Consider a two-dimensional homogeneous poroelastic medium saturated with a mixture of water and gas in a solid deformable skeleton. The properties of the skeleton and pore fluid are given in Table 1.

The simulations were performed for the square computational domain $(x, y) \in [-a, a] \times [-b, b]$ with $a = b = 0.01\ m$. The nodes of the uniform finite grid $2000 * 2000$ have a spatial discretization of $1 \cdot 10^{-5}\ m$ and time step of $1 \cdot 10^{-9}\ s$.

The wavefield is exited by the forces applied to the domain boundaries as follows:

$$\sigma_{11}|_{x=-a} = F_1^1(t),\ \sigma_{12}|_{x=-a} = 0,\ W_1^1|_{x=-a} = 0,\ W_2^1|_{x=-a} = 0, \tag{20}$$

$$\sigma_{11}|_{x=a} = 0,\ \sigma_{12}|_{x=a} = 0,\ W_1^1|_{x=a} = 0,\ W_2^1|_{x=a} = 0 \tag{21}$$

$$\sigma_{22}|_{x=-b} = 0,\ \sigma_{12}|_{x=-b} = 0,\ W_1^2|_{x=-b} = 0,\ W_2^2|_{x=-b} = 0, \tag{22}$$

$$\sigma_{22}|_{x=b} = 0,\ \sigma_{12}|_{x=b} = 0,\ W_1^2|_{x=b} = 0,\ W_2^1|_{x=b} = 0. \tag{23}$$

where $F_1^1(t)$ is a Gaussian pulse function with source frequency $f_0 = 10^6$ and time delay $t_0 = 1/f_0\ s$:

$$F_1^1(t) = exp[-(\pi f_0(t - t_0))^2], \tag{24}$$

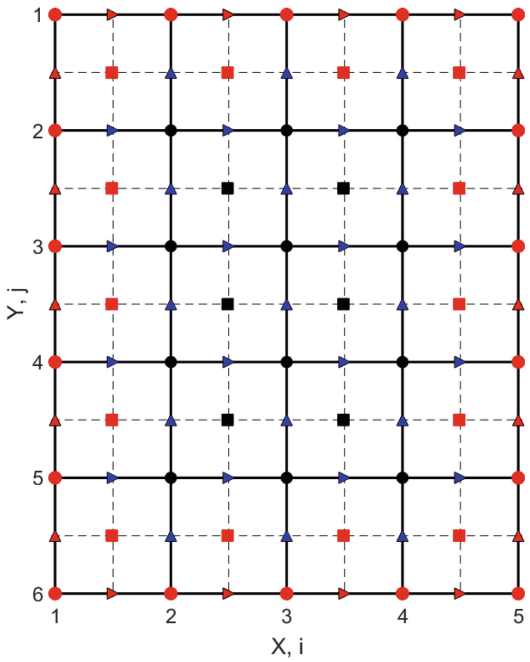

Fig. 2. Nodes involved in approximating the boundary conditions (11)–(14) on the staggered grid. The nodes where specific boundary conditions are defined are highlighted in red colour. (Color figure online)

The boundary conditions are chosen so as to excite a plane wave propagating from left to right along the x-axis.

This simple test allows us to evaluate both the seismic wave propagation velocities in porous media as a function of the composition of volume fractions, and the correctness of the numerical realization of the boundary conditions themselves.

Depending on the chosen phases, the model (1) can describe a purely elastic medium with given seismic velocities, such as pure solid ($\alpha_1^0 = 0$, $\alpha_2^0 = 0$, $\alpha_3^0 = 1$), pure air ($\alpha_1^0 = 1$, $\alpha_2^0 = 0$, $\alpha_3^0 = 0$) or pure water ($\alpha_1^0 = 0$, $\alpha_2^0 = 1$, $\alpha_3^0 = 0$), or a porous medium containing one or two fluid phases in different proportions.

Consider a homogeneous poroelastic medium containing a solid deformable skeleton saturated with 70% water ($\alpha_1^0 = 0$, $\alpha_2^0 = 0.7$, $\alpha_3^0 = 0.3$). The properties of the skeleton (Solid phase) and the water (Fluid2) are given in Table 1.

For the chosen boundary conditions we should obtain two plane waves propagating from left to right along the x-axis. The velocities of these waves should correspond to the velocities calculated by formulae (4), (5).

Figure 3 shows numerical snapshots of the wavefield component V^1 at times $t = 4 * 10^{-6}$ s and $t = 9 * 10^{-6}$ s. The amplitude of the corresponding plain wave is indicated by the red line at the bottom of the snapshots.

As expected, fast and slow (in the Biot regime) plane compression waves are observed in Fig. 3. The numerically estimated velocities 1950 m/s for the fast P-wave and 280 m/s for the slow P-wave agree well with the values obtained from the velocity estimation formulae (4), (5), which are 1954 m/s and 277 m/s respectively.

Table 1. Physical parameters used for simulation in homogeneous test cases.

State	Property	Parameters	Value	Unit
Fluid1: (air)	Fluid density	ρ_1^0	1.225	kg/m^3
	Sound velocity	c_1	330	m/s
	Bulk modulus	$K_1 = \rho_1^0 c_1^2$	0.00013	GPa
Fluid2: (water)	Fluid density	ρ_2^0	1040	kg/m^3
	Sound velocity	c_2	1500	m/s
	Bulk modulus	$K_2 = \rho_2^0 c_2^2$	2.34	GPa
Solid phase:	Solid density	ρ_3^0	2500	kg/m^3
	P-wave velocity	v_p	6155	m/s
	S-wave velocity	v_s	3787	m/s
	Bulk velocity	c_s	4332	m/s
	Bulk modulus	$K_3 = \rho_3^0 c_s^2$	46.91	GPa
	Shear modulus	$\mu = \rho_3^0 v_s^2$	35.85	GPa

3.4 Test 2

Let us consider two numerical test problems in a homogeneous poroelastic medium containing in the center of the domain a homogeneous purely elastic inclusion in the form of a circle of radius 0.1 with material parameters $v_p = 6000$ m/s, $v_s = 4000$ m/s, $\rho = 2500$ kg/m^3. The domain size and finite difference grid are the same as in Test1.

In the first simulation the surrounding homogeneous poroelastic medium is the same as in Test 1, i.e. it consists of a solid skeleton and water ($\alpha_1^0 = 0$, $\alpha_2^0 = 0.7$, $\alpha_3^0 = 0.3$), while in the second simulation we consider a porous medium consisting of a solid skeleton with a mixture of two fluid phases, 10% air and 70% water ($\alpha_1^0 = 0.1$, $\alpha_2^0 = 0.7$, $\alpha_3^0 = 0.2$).

The results of calculations are shown in Figs. 4 and 5. As can be seen from the figures, the presence of an additional air phase in the medium significantly reduces the wave velocity. According to formulas (4), (5), these velocities should

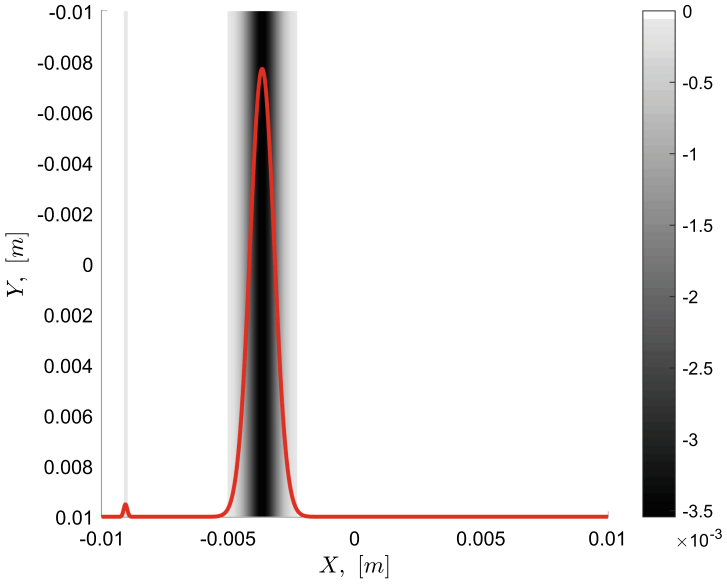

(a) $t = 4 * 10^{-6}\ s$

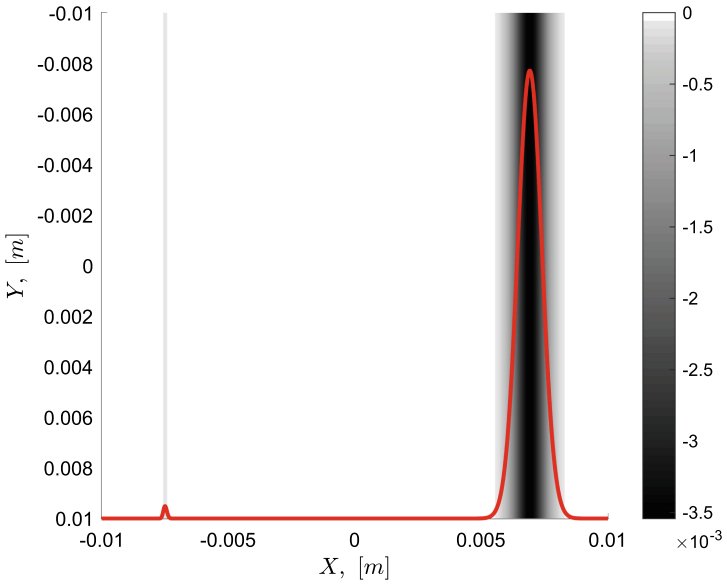

(b) $t = 9 * 10^{-6}\ s$

Fig. 3. Snapshots of the wavefield velocity V^1 at times $t = 4 * 10^{-6}\ s$ and $t = 9 * 10^{-6}\ s$. The amplitudes of the corresponding plane waves are indicated by the red line at the bottom of the images. (Color figure online)

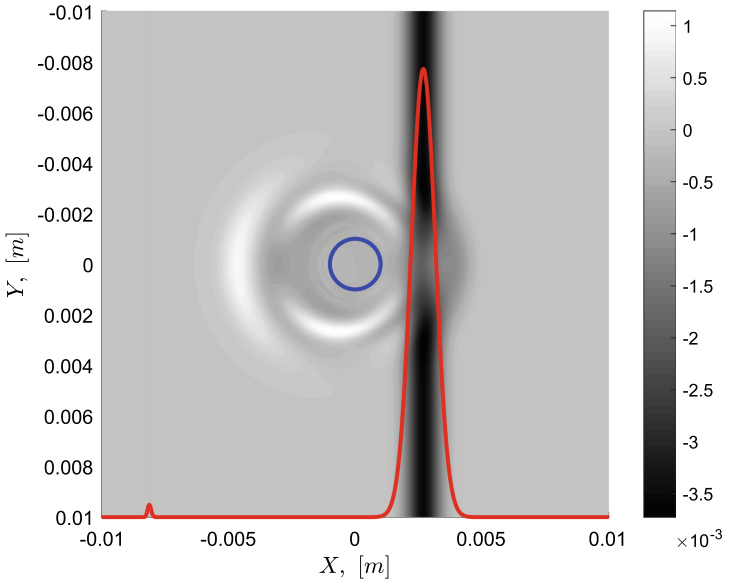

(a) $t = 8 \cdot 10^{-6}\ s$

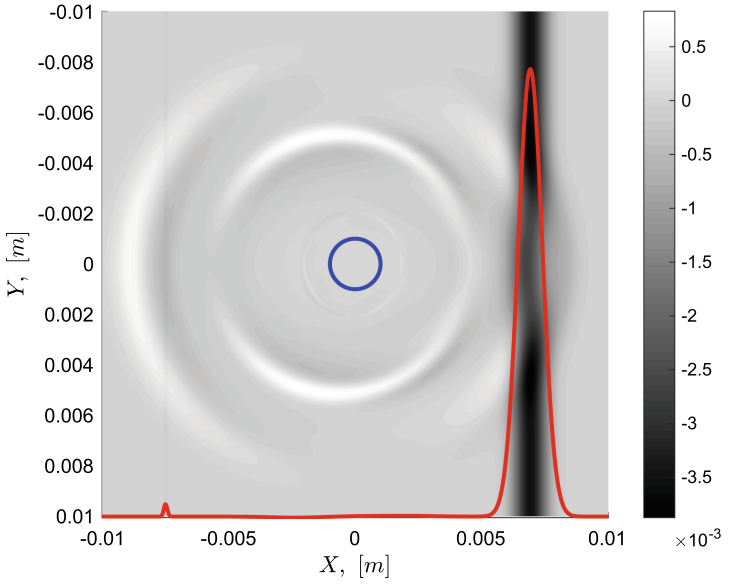

(b) $t = 10^{-5}\ s$

Fig. 4. Snapshots of the wavefield velocity V^1 at times $t = 8 \cdot 10^{-6}\ s$ and $t = 10^{-5}\ s$ for the surrounding homogeneous poroelastic medium consisting of a solid skeleton saturated with water ($\alpha_1^0 = 0, \alpha_2^0 = 0.7, \alpha_3^0 = 0.3$). The amplitudes of the corresponding plane waves are indicated by the red line at the bottom of the images. (Color figure online)

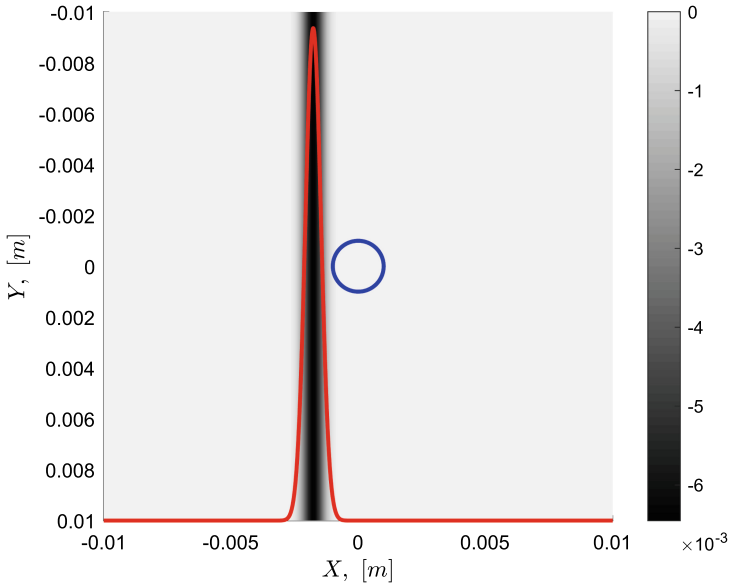

(a) $t = 8 \cdot 10^{-6}\ s$

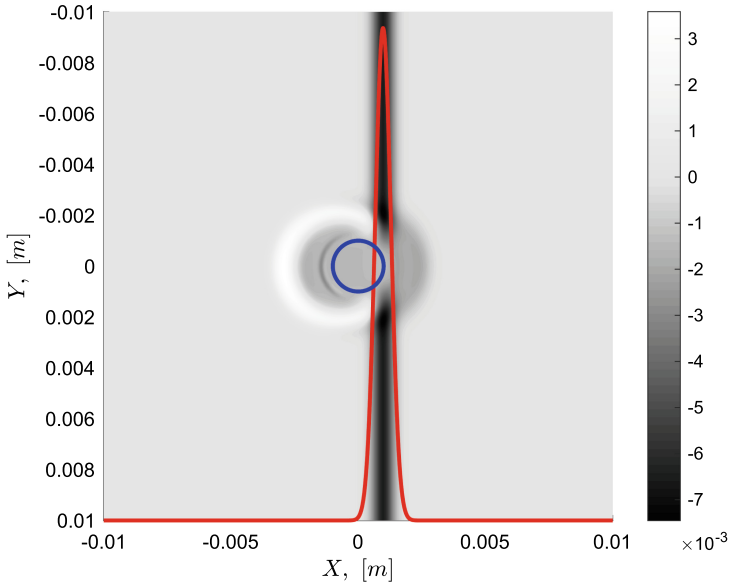

(b) $t = 10^{-5}\ s$

Fig. 5. Snapshots of the wavefield velocity V^1 at times $t = 8 \cdot 10^{-6}\ s$ and $t = 10^{-5}\ s$ for the surrounding homogeneous poroelastic medium consisting of a solid skeleton saturated with a mixture of air and water ($\alpha_1^0 = 0.1$, $\alpha_2^0 = 0.7$, $\alpha_3^0 = 0.2$). The amplitudes of the corresponding plane waves are indicated by the red line at the bottom of the images. (Color figure online)

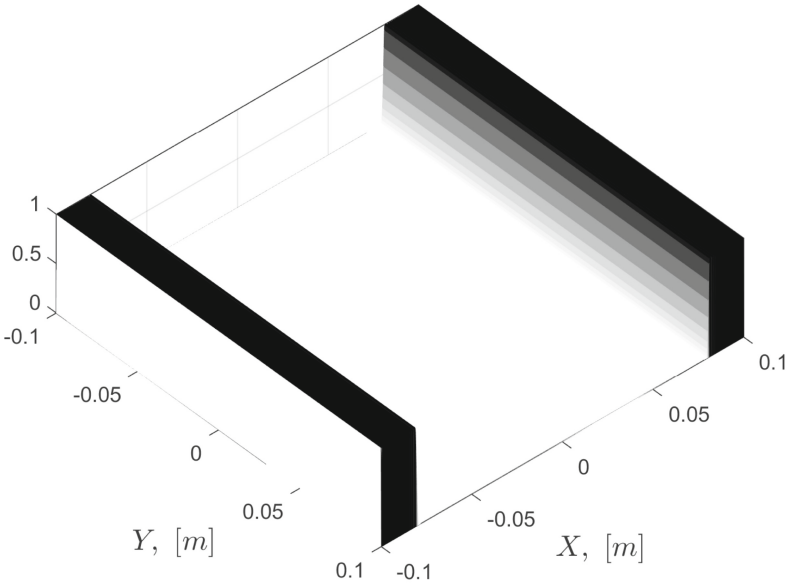

(a) $t = 2 \cdot 10^{-6}\ s$

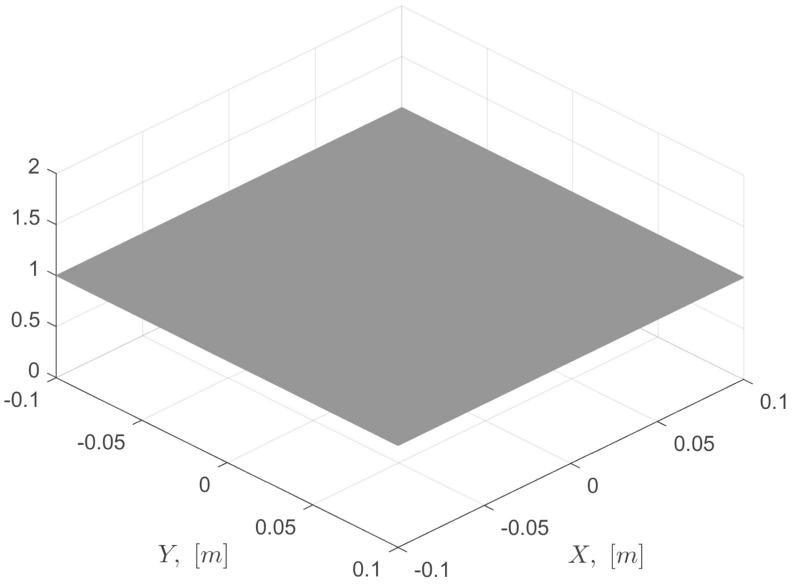

(b) $t = 10^{-4}\ s$

Fig. 6. Snapshots of the stress tensor component σ_{11} at times $t = 2 \cdot 10^{-6}\ s$ and $t = 10^{-4}\ s$.

be 1032 m/s for a fast P-wave and 329.5 m/s for a slow P-wave. Numerical estimates of the velocities give values that agree well with the theoretical estimates.

Note that when plane waves are reflected from a circular object placed in a poroelastic medium, not only longitudinal waves but also transverse waves are generated, which can be clearly seen in Fig. 4.

3.5 Test 3

This test shows how a problem of static equilibrium of poroelastic body can be solved using a dynamic poroelasticity system (1) with given boundary conditions using an iterative relaxation method. This approach has been used, for example, to estimate the elastic properties of rock samples from their tomographic images [9].

We propose to find a solution of static poroelastic problem

$$\frac{\partial \sigma_{ik}}{\partial x_k} = 0, \quad i,k = 1,2,3, \tag{25}$$

$$\sigma_{ik} = \lambda(\varepsilon_{11} + \varepsilon_{22} + \varepsilon_{33})\delta_{ik} + 2\mu\varepsilon_{ik}. \tag{26}$$

with boundary conditions (11)–(14) by finding the steady-state solution of the system (1) by adding dissipative relaxation terms $\beta V^i, \beta W_1^i, \beta W_2^i$ to the equations of motion:

$$\rho_0 \frac{\partial V^i}{\partial t} + \beta V^i + \frac{\partial P}{\partial x_i} - \frac{\partial \Sigma_{ik}}{\partial x_k} = 0, \tag{27a}$$

$$\frac{\partial W_1^i}{\partial t} + \beta W_1^i + \left(\frac{1}{\rho_1^0} - \frac{1}{\rho_3^0}\right)\frac{\partial P}{\partial x_i} = 0, \tag{27b}$$

$$\frac{\partial W_2^i}{\partial t} + \beta W_2^i + \left(\frac{1}{\rho_2^0} - \frac{1}{\rho_3^0}\right)\frac{\partial P}{\partial x_i} = 0, \tag{27c}$$

where β is a small positive constant chosen empirically. The convergence to the static problem follows from the virial theorem [10], §10.

As an example, consider the problem (25)–(26) with boundary conditions (11)–(14), where we assume the functions $F_1^1(t) = F_2^1(t) = 1$, $F_3^1(t) = F_4^1(t) = 0$, $F_1^2(t) = F_2^2(t) = F_3^2(t) = F_4^2(t) = 0$. In this case, the exact solution of the problem is $\sigma_{11} = 1$.

The simulation was carried out using the computational domain and parameters of the medium presented in Test 1 of this section. The boundary conditions were approximated according to the scheme in Fig. 2 of Sect. 3.2.

Figure 6 shows snapshots of the stress tensor component σ_{11} at two time instants. The upper snapshot in Fig. 6 shows the wavefield at the moment of its excitation by a constant stress set at the lateral boundaries of the domain. After the wavefield has propagated inside the domain, we switch on damping parameter ($\beta = 0.001$) and the process starts to converge to the solution of the stationary problem $\sigma_{11} = 1$.

This iterative approach can be useful in the case of a general three dimensional problem, since direct methods for solving static problems require a large amount of RAM.

4 Conclusion

A numerical method for solving some boundary value problems for a Hyperbolic Thermodynamically Compatible (HTC) model of a deformable porous medium saturated with a mixture of two liquids has been developed. The method is based on a finite difference scheme on a staggered grid, for which the formulated basic equations are perfectly suited. A set of test cases for wave propagation in rectangular domain is solved, including a test problem for obtaining a steady-state solution by solving a non-stationary system. The developed method can be applied to the analysis of wavefields in areas with a complex structure, as well as to the evaluation of the effective elastic moduli of a saturated porous medium - a problem that we plan to investigate.

Acknowledgments. The development of the mathematical model by E. Romenski was financially supported by the Russian Science Foundation (Project No. 19-77-20004), the development of the numerical method and the simulations performed by G. Reshetova was carried out under state contract with ICMMG SB RAS FWNM-2025-0004.

Disclosure of Interests. The authors declare that they have no known competing financial interests or personal relationships that could have appeared to influence the work reported in this article.

References

1. Biot, M. A.: Theory of propagation of elastic waves in fluid-saturated porous solid. I. Low-frequency range. J. Acoust. Soc. Am. **28**(2), 168–178 (1956)
2. Biot, M. A.: Theory of propagation of elastic waves in a fluid-saturated porous solid. II. Higher frequency range. J. Acoust. Soc. Am. **28**(2), 179–191 (1956)
3. Carcione, J.M., Morency, C., Santos, V.: Computational poroelasticity - a review. Geophysics **75**(5), 75A229-75A243 (2010)
4. Romenski, E., Reshetova, G., Peshkov, I., Dumbser, M.: Modeling wavefields in saturated elastic porous media based on thermodynamically compatible system theory for two-phase solid-fluid mixtures. Comput. Fluids **206**, 104587 (2020)
5. Reshetova, G., Romenski, E.: Diffuse interface approach to modeling wavefields in a saturated porous medium. Appl. Math. Comput. **398**, 125978 (2021)
6. Romenski, E., Reshetova, G., Peshkov, I.: Two-phase hyperbolic model for porous media saturated with a viscous fluid and its application to wavefield simulation. Appl. Math. Model. **106**, 567–600 (2022)
7. Reshetova, G., Romenski, E.: Modeling of temperature-dependent wave fields in deformable porous media saturated with fluid. Numer. Anal. Appl. **17**(4), 358–371 (2024)
8. Reshetova, G., Romenski, E.: Modeling the variability of seismic properties of frozen multiphase media depending on temperature. Siberian Electron. Math. Rep. **21**(2), B203–B231 (2024)
9. Reshetova, G., Khachkova, T.: Parallel numerical method to estimate the effective elastic moduli of rock core samples from 3D tomographic images. In: Dimov, I., Farago, I., Vulkov, L. (eds.) FDM 2018. LNCS, vol. 11386, pp. 452–460. Springer, Cham (2019). https://doi.org/10.1007/978-3-030-11539-5_52

10. Landau, L.D., Lifshitz, E.M.: Mechanics. Nauka, Moscow (1988)
11. Peshkov, I., Pavelka, M., Romenski, E., Grmela, M.: Continuum mechanics and thermodynamics in the Hamilton and the Godunov-type formulations. Continuum Mech. Thermodyn. **30**(6), 1343–1378 (2018). https://doi.org/10.1007/s00161-018-0621-2
12. Virieux, J.: P-SV wave propagation in heterogeneous media: velocity-stress finite-difference method. Geophysics **51**(1), 889–901 (1986)
13. Levander, A.R.: Fourth-order finite-difference P-SV seismograms. Geophysics **53**(11), 1425–1436 (1988)
14. Samarskii, A.A.: The Theory of Difference Schemes. CRC Press, Boca Raton (2001)
15. Moczo, P., Kristek, J., Vavrycuk, V., Archuleta, R.J., Halada, L.: 3D heterogeneous staggered-grid finite-difference modeling of seismic motion with volume harmonic and arithmetic averaging of elastic moduli and densities. Bull. Seismol. Soc. Am. **92**(8), 3042–3066 (2002)